PHYSICS AND CHEMISTRY OF SOLID STATE
V. 25, No. 3 (2024) pp. 513-519
Section: Chemistry

DOI: 10.15330/pcss.25.3.513-519

Vasyl Stefanyk Precarpathian National University

ФІЗИКА І ХІМІЯ ТВЕРДОГО ТІЛА
Т. 25, № 3 (2024) С. 513-519
Хімічні науки

PACS: 61.66.Fn

ISSN 1729-4428 (Print)
ISSN 2309-8589 (Online)

O. Smitiukh, O. Marchuk

The effect of substitution rare earth metal on crystal structure and properties of quaternary $La_{4-4x}R_{4x}Ge_3S_{12}$ (R – Er, Ho, Y, Dy, Tb) sulfide

Lesya Ukrainka Volyn National University, Lutsk, Ukraine, Smitiukh.Oleksandr@vnu.edu.ua

Establishing relationships between the distribution of atoms in a crystalline unit cell and the properties of phases is an important issue directly related to the application of functional materials. In this work, we present an analysis of the crystalline structure, chemical bonds, and prediction of material properties using the example of tetragonal phases $La_{4-4x}R_{4x}Ge_3S_{12}$ (R - Er, Ho, Y, Dy, Tb), which crystallize in space group *R*3*c*. The presence of rare earth elements with high coordination in the first coordination sphere is a significant contribution to changing properties, particularly thermoelectric properties. This creates the possibility of increasing the entropy factor and, as a result, improving the thermoelectric characteristics. The parameters of the elementary cell of the initial ternary phase $La_4Ge_3S_{12}$ decrease at a ratio of 1La:1R (R - Tb, Dy, Ho, Er) in the site 6*a* and 18*b*. In the Er-containing phase, the lowest distortion index for the [M1 8S] polyhedron, while in the [M1 9S] polyhedron it significantly increases. Additionally, the formation of "columns" from polyhedra [Ge2 6S] creates the possibility of directional excitation in one direction, which can also have a significant impact on material properties. Overall, the obtained non-symmetric materials may be promising for nonlinear optics.

Keywords: distortion factor; crystalline structure; rare earth metals; elementary cell; tetragonal sulfides.

Received 6 March 2024; Accepted 17 July 2024.

Introduction

The crystal structure and properties of materials play a crucial role in determining their potential applications in various fields. In the study of quaternary sulfides, the effect of substitution rare earth metal on the crystal structure and properties [1] of *R*3*c* quaternary $La_{4-4x}R_{4x}Ge_3S_{12}$ (R – Er, Ho, Y, Dy, Tb) sulfides has garnered significant attention. Substitution, the process of replacing one element with another in a crystal lattice, can lead to changes in the structural arrangement of atoms and, consequently, influence the physical and chemical properties of the material [2]. Substitution of rare earth elements can lead to changes in the crystal structure of *R*3*c* quaternary $La_{4-4x}R_{4x}Ge_3S_{12}$ (R – Er, Ho, Y, Dy, Tb) sulfides as it is in the work [3]. The size, charge, and chemical properties of the substituted rare earth element can influence the arrangement of atoms in the crystal lattice, leading to structural distortions, changes in bond lengths, and alterations in symmetry [4].

Substitution of rare earth elements may introduce defects in the crystal structure of *R*3*c* quaternary $La_{4-4x}R_{4x}Ge_3S_{12}$ (R – Er, Ho, Y, Dy, Tb) sulfides. These defects can affect the electronic and ionic conductivity, thermal stability, and mechanical properties of the material [5]. The magnetic, optical, electrical, and thermal properties of the material can be modified by varying the rare earth element composition [6]. This tuning can be exploited for applications in magneto-optical devices, sensors, catalysis, and energy storage. By selecting appropriate rare earth elements with specific properties, such as high magnetic moment or chemical stability, the material's overall performance can be improved for targeted applications.

This article explores the impact of substitution on the crystal structure and properties of *R*3*c* quaternary $La_{4-4x}R_{4x}Ge_3S_{12}$ (R – Er, Ho, Y, Dy, Tb) sulfides, shedding light on how these modifications can be harnessed to tailor

the characteristics of these materials for specific applications.

I. Experimental details

In the present work, we obtained the samples for investigation from high-purity elements. The total mass of a sample was 1 g. Co-melting of the elements was held in evacuated ampoules (residual pressure 10^{-2} Pa) in an MP-30 programmable electric muffle furnace in two stages. The first stage was heating to 1423 K (heating rate 12 K/h); exposure to 1423 K for 4 h; cooling to room temperature (cooling rate 12 K/h). At the second stage to obtain homogeneous samples, pre-synthesized ingots were ground into powder and pressed into tablets. These were again placed in evacuated containers, reheated to 773 K at the rate of 12 K/h, annealed at this temperature for 500 h, and quenched into room-temperature water (without depressurizing the containers).

Phase identification was performed with a DRON-4-13 X-ray diffractometer using CuKα-radiation ($\Delta 2\Theta = 0.02^o$, 2Θ range 10 - 100^o) with Bragg-Brentano geometry. Rietveld refinement of the crystal structure was performed in the WinCSD program package [7]. Visualization of the crystal structure utilized VESTA program [8].

II. Results and discussion

2.1. Crystal structure of $La_{4-4x}R_{4x}Ge_3S_{12}$ (R – Er, Ho, Y, Dy, Tb).

According to our investigation [9-11] the $La_{4-4x}R_{4x}Ge_3S_{12}$ (x = 0 ÷ 0.75) (Fig. 1) solid solutions based on $La_4Ge_3S_{12}$ ternary phase (ST *own*; Symbol Pearson *hR* 38.161; SG *R*3*c*) exist in the quasi-ternary $La_2S_3 – R_2S_3 – GeS_2$ (R – Er, Ho, Y, Dy, Tb) system. The range of the solid solutions is following:

$La_{4-4x}Er_{4x}Ge_3S_{12}$ is up to 62 mol. % of "$Er_4Ge_3S_{12}$";
$La_{4-4x}Ho_{4x}Ge_3S_{12}$ – up to 60 mol. % of "$Ho_4Ge_3S_{12}$";
$La_{4-4x}Y_{4x}Ge_3S_{12}$ – up to 75 mol. % of "$Y_4Ge_3S_{12}$";
$La_{4-4x}Dy_{4x}Ge_3S_{12}$ – up to 70 mol. % of "$Dy_4Ge_3S_{12}$";
$La_{4-4x}Tb_{4x}Ge_3S_{12}$ – up to 72 mol. % of "$Tb_4Ge_3S_{12}$".

The change of the lattice parameter in the structure is presented in Table 1. It is worth noticing that the parameter of the $La_{4-4x}Dy_xGe_3S_{12}$ (x = 0 ÷ 0.70) solid solution has the widest Δ (a, c and V) (Fig. 1): *a* decreases from 1.9400 nm to 1.9137 nm, *c* - from 0.8100 nm to 0.7829 nm, volume of the lattice cell decreases from 2.6400 nm^3 to 2.4847 nm^3.

The crystal structure of the separate compositions ($La_{2,16}Er_{1,84}Ge_3S_{12}$, $La_{2,25}Ho_{1,75}Ge_3S_{12}$, $La_{2,64}Dy_{1,36}Ge_3S_{12}$ and $La_{2,02}Tb_{1,98}Ge_3S_{12}$) of $R_{4x}La_{4-4x}Ge_3S_{12}$ solid solutions is investigated by X-ray single crystal diffraction and

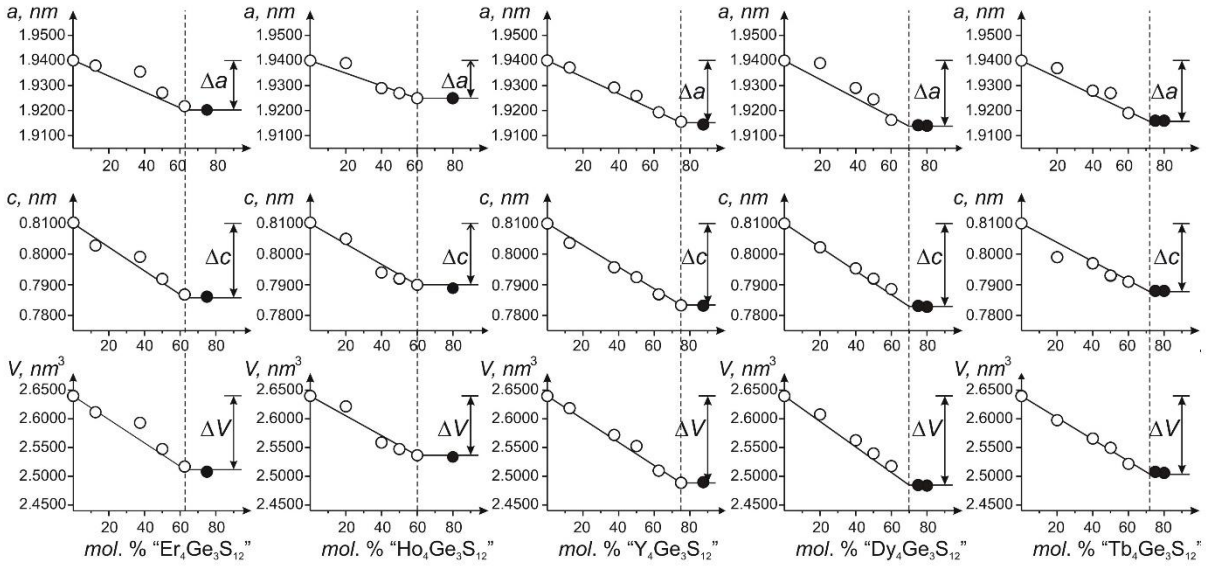

Fig. 1. The change of the lattice parameter in the structure of the $La_{4-4x}R_{4x}Ge_3S_{12}$ (R – Er, Ho, Y, Dy, Tb) solid solutions.

Table 1.

The change of the lattice parameter in the structure of the $La_{4-4x}R_{4x}Ge_3S_{12}$ (R – Er, Ho, Y, Dy, Tb) solid solutions

Composition	*a*, nm	Δ*a*, nm	*c*, nm	Δ*c*, nm	*V*, nm^3	Δ*V*, nm^3
$La_4Ge_3S_{12}$	1.9400	–	0.8100	–	2.6400	–
$La_{4-4x}Er_{4x}Ge_3S_{12}$ (x = 0.62)	1.9203	0.0197	0.7858	0.0242	2.5117	0.1283
$La_{4-4x}Ho_{4x}Ge_3S_{12}$ (x = 0.60)	1.9149	0.0251	0.7900	0.0200	2.5366	0.1034
$La_{4-4x}Y_{4x}Ge_3S_{12}$ (x = 0.75)	1.9152	0.0248	0.7834	0.0266	2.4886	0.1514
$La_{4-4x}Dy_{4x}Ge_3S_{12}$ (x = 0.70)	1.9137	0.0263	0.7829	0.0271	2.4847	0.1553
$La_{4-4x}Tb_xGe_3S_{12}$ (x = 0.72)	1.9157	0.0243	0.7878	0.0222	2.5035	0.1365

some of the composition are studied by X-ray powder method.

Details of the experiment, atomic displacement parameters refined in the anisotropic approximation ($La_{2,16}Er_{1,84}Ge_3S_{12}$, $La_{2,25}Ho_{1,75}Ge_3S_{12}$, $La_{2,64}Dy_{1,36}Ge_3S_{12}$ i $La_{2,02}Tb_{1,98}Ge_3S_{12}$) and interatomic distances are given in the Table 2-7.

$La_{2,16}Er_{1,84}Ge_3S_{12}$ (Table 3). The distance between M1 {0.20 La + 0.80 Er} and Sulfur atoms in the [M1 6S] trigonal prism are within $\delta(M1\text{-}S)_{min}$ = 0.27904(19) nm to $\delta(M1\text{-}S)_{max}$ = 0.2806(2) nm. The distance between M2 {0.65 La + 0.35 Er} and Sulfur atoms in the [M2 7S] trigonal prism with additional atom is within $\delta(M2\text{-}S)_{min}$ = 0.28491(18) nm to $\delta(M2\text{-}S)_{max}$ = 0.30007(19) nm. The distance of Ge-S in the [Ge 4S] is $\delta(Ge\text{-}S)_{min}$ = 0.2195(2) nm to $\delta(Ge\text{-}S)_{max}$ = 0.22466(19) nm.

$La_{2,25}Ho_{1,75}Ge_3S_{12}$ (Table 4). The distance between M1 {0.22 La + 0.78 Ho} and Sulfur atoms in the [M1 6S] trigonal prism is $\delta(M1\text{-}S)_{min}$ = 0.28080(15) nm to $\delta(M1\text{-}S)_{max}$ = 0.28200(16) nm. The distance M2 {0.68 La + 0.32 Ho} – S in the [M2 7S] trigonal prism with additional atom is within $\delta(M2\text{-}S)_{min}$ = 0.28512(15) nm to $\delta(M2\text{-}S)_{max}$ = 0.30176(15) nm. The distance of Ge-S in the [Ge 4S] is $\delta(Ge\text{-}S)_{min}$ = 0.21958(16) nm to $\delta(Ge\text{-}S)_{max}$ = 0.22461(16) nm.

$La_2Y_2Ge_3S_{12}$ (Table 5). The distance of M1 {0.09 La + 0.91 Y} - S in the [M1 6S] trigonal prism is $\delta(M1\text{-}S)_{min}$ = 0.2794 nm to $\delta(M1\text{-}S)_{max}$ = 0.2860 nm. The distance of M2 {0.63 La + 0.37 Y} - S in the [M2 7S] trigonal prism with additional atom is within $\delta(M2\text{-}S)_{min}$= 0,2787(9) nm to $\delta(M2\text{-}S)_{max}$= 0,3087(9) nm. The distance of Ge-S in the [Ge 4S] is $\delta(Ge\text{-}S)_{min}$ = 0.2160(8) nm to $\delta(Ge\text{-}S)_{max}$ = 0.2303(10) nm.

$La_{2,64}Dy_{1,36}Ge_3S_{12}$ (Table 6). The distance of M1 {0.35 La + 0.65 Dy} - S in the [M1 6S] trigonal prism is $\delta(M1\text{-}S)_{min}$ = 0.28260(18) nm to $\delta(M1\text{-}S)_{max}$ = 0.28342(18) nm. The distance of M2 {0.76 La + 0.24 Dy} - S in the [M2 7S] trigonal prism with additional atom is within $\delta(M2\text{-}S)_{min}$ = 0.28539(17) nm to $\delta(M2\text{-}S)_{max}$ = 0.30343(18) nm. The distance of Ge-S in

Table 2.

The lattice parameter of the compositions $La_{4-4x}R_{4x}Ge_3S_{12}$ (R – Er, Ho, Y, Dy, Tb)

Composition	Method		Lattice parameter, nm		
	⊗ (p)	⊕ (s)	*a*, nm	*b*, nm	*c*, nm
$La_{2,16}Er_{1,84}Ge_3S_{12}$		⊕ (s)	1.92165(4)	1.92165(4)	0.78757(2)
$La_{2,25}Ho_{1,75}Ge_3S_{12}$		⊕ (s)	1.92448(6)	1.92448(6)	0.79096(4)
$La_2Y_2Ge_3S_{12}$	⊗ (p)		1.92587(9)	1.92587(9)	0.79121(5)
$La_{2,64}Dy_{1,36}Ge_3S_{12}$		⊕ (s)	1.92868(5)	1.92868(5)	0.79498(2)
$La_{2,02}Tb_{1,98}Ge_3S_{12}$		⊕ (s)	1.92627(5)	1.92627(5)	0.79263(2)

⊗ (p) – powder; ⊕ (s) – single crystal

Table 3.

The atomic displacement parameters in the anisotropic approximation of $La_{2,16}Er_{1,84}Ge_3S_{12}$

Atom	Site	Occ.	*x*/*a*	*y*/*b*	*z*/*c*	$U_{экв}\times10^2$ (nm^2)
La1	6*a*	0.20	0	0	0	0.0156(2)
Er1	6*a*	0.80	0	0	0	0.0156(2)
La2	18*b*	0.65	0.00561(2)	0.23269(2)	0.21091(5)	0.01575(13)
Er2	18*b*	0.35	0.00561(2)	0.23269(2)	0.21091(5)	0.01575(13)
Ge	18*b*	1.0	0.19819(4)	0.18583(4)	0.16050(9)	0.0106(2)
S1	18*b*	1.0	0.28665(10)	0.17814(12)	-0.0030(3)	0.0197(4)
S2	18*b*	1.0	0.11948(11)	0.05862(10)	0.2486(3)	0.0156(4)
S3	18*b*	1.0	0.11378(11)	0.20200(11)	0.0004(2)	0.0159(4)
S4	18*b*	1.0	0.27482(11)	0.27028(11)	0.3586(2)	0.0174(4)

Table 4.

The atomic displacement parameters in the anisotropic approximation of $La_{2,25}Ho_{1,75}Ge_3S_{12}$

Atom	Site	Occ.	*x*/*a*	*y*/*b*	*z*/*c*	$U_{экв}\times10^2$ (nm^2)
La1	6*a*	0.22	0	0	0	0.01514(17)
Ho1	6*a*	0.78	0	0	0	0.01514(17)
La2	18*b*	0.68	0.00512(2)	0.23235(2)	0.20972(4)	0.01557(10)
Ho2	18*b*	0.32	0.00512(2)	0.23235(2)	0.20972(4)	0.01557(10)
Ge	18*b*	1.0	0.19840(3)	0.18600(4)	0.15939(7)	0.01083(17)
S1	18*b*	1.0	0.28676(9)	0.17798(10)	-0.0029(19)	0.0188(4)
S2	18*b*	1.0	0.12012(9)	0.05927(9)	0.2489(2)	0.0156(3)
S3	18*b*	1.0	0.11377(9)	0.20170(10)	0.00018(18)	0.0164(3)
S4	18*b*	1.0	0.27474(10)	0.27032(9)	0.35681(18)	0.0171(4)

Table 5.

The atomic displacement parameters in the anisotropic approximation of $La_2Y_2Ge_3S_{12}$

Atom	Site	Occ.	*x*/*a*	*y*/*b*	*z*/*c*	$U_{екв}\times10^2$ (nm^2)
La1	6*a*	0.09	0	0	0	0.61(6)
Y1	6*a*	0.91	0	0	0	0.61(6)
La2	18*b*	0.63	0.0046(2)	0.2302(1)	0.2083(5)	0.38(3)
Y2	18*b*	0.37	0.0046(2)	0.2302(1)	0.2083(5)	0.38(3)
Ge	18*b*	1.0	0.1964(2)	0.1862(2)	0.1638(5)	0.88(9)
S1	18*b*	1.0	0.1581(4)	0.3758(4)	0.1721(11)	0.4(2)
S2	18*b*	1.0	0.1211(4)	0.0635(4)	0.2440(9)	0.4(3)
S3	18*b*	1.0	0.1116(5)	0.2013(4)	1.0048(9)	0.3(3)
S4	18*b*	1.0	0.3928(4)	0.0574(4)	0.1916(10)	1.0(2)

Table 6.

The atomic displacement parameters in the anisotropic approximation of $La_{2,64}Dy_{1,36}Ge_3S_{12}$

Atom	Site	Occ.	*x*/*a*	*y*/*b*	*z*/*c*	$U_{екв}\times10^2$ (nm^2)
La1	6*a*	0.35	0	0	0	0.01332(19)
Dy1	6*a*	0.65	0	0	0	0.01332(19)
La2	18*b*	0.76	0.23180(2)	0.00440(2)	0.29217(5)	0.01431(11)
Dy2	18*b*	0.24	0.23180(2)	0.00440(2)	0.29217(5)	0.01431(11)
Ge	18*b*	1.0	0.18617(4)	0.19870(4)	0.34239(8)	0.01012(19)
S1	18*b*	1.0	0.17763(11)	0.28681(10)	0.5037(2)	0.0167(4)
S2	18*b*	1.0	0.06020(10)	0.12063(10)	0.2507(2)	0.0143(4)
S3	18*b*	1.0	0.20135(11)	0.11384(10)	0.5012(2)	0.0153(4)
S4	18*b*	1.0	0.27045(10)	0.27455(11)	0.1456(2)	0.0154(4)

Table 7.

The atomic displacement parameters in the anisotropic approximation of $La_{2,02}Tb_{1,98}Ge_3S_{12}$

Atom	Site	Occ.	*x*/*a*	*y*/*b*	*z*/*c*	$U_{екв}\times10^2$ (nm^2)
La1	6*a*	0.13	0	0	0	0.01507(16)
Tb1	6*a*	0.87	0	0	0	0.01507(16)
La2	18*b*	0.63	0.23214(2)	0.00481(2)	0.29107(5)	0.01602(10)
Tb2	18*b*	0.37	0.23214(2)	0.00481(2)	0.29107(5)	0.01602(10)
Ge	18*b*	1.0	0.18612(3)	0.19854(3)	0.34133(7)	0.01108(17)
S1	18*b*	1.0	0.17791(9)	0.28680(8)	0.50334(19)	0.0181(3)
S2	18*b*	1.0	0.05962(9)	0.12026(9)	0.2509(2)	0.0156(3)
S3	18*b*	1.0	0.20154(9)	0.11378(9)	0.50011(19)	0.0162(3)
S4	18*b*	1.0	0.27040(9)	0.27465(9)	0.14436(18)	0.0171(3)

the [Ge 4S] is $\delta(Ge\text{-}S)_{min}$ = 0.21993(19) nm to $\delta(Ge\text{-}S)_{max}$ = 0.22456(18) nm.

$La_{2,02}Tb_{1,98}Ge_3S_{12}$ (Table 7). The distance of M1 {0.13 La + 0.87 Tb} - S in the [M1 6S] trigonal prism is $\delta(M1\text{-}S)_{min}$ = 0.28146(15) nm to $\delta(M1\text{-}S)_{max}$ = 0.28250(16) nm. The distance of M2 {0.63 La + 0.37 Tb} - S in the [M2 7S] trigonal prism with additional atom is within $\delta(M2\text{-}S)_{min}$ = 0.28515(15) nm to $\delta(M2\text{-}S)_{max}$ = 0.30266(15) nm. The distance of Ge-S in the [Ge 4S] is $\delta(Ge\text{-}S)_{min}$ = 0.21960(16) nm to $\delta(Ge\text{-}S)_{max}$ = 0.22472(16) nm.

2.2. The $La_2S_3 – R'_2S_3 – GeS_2$ systems.

The $La_2S_3 – R'_2S_3 – GeS_2$ (R' – Tb, Dy, Y, Ho, Er) systems are the one of the possible tetrahedron of La – R' – Ge – S (Fig. 2).

The $La_{4-4x}Er_xGe_3S_{12}$ (x = 0 - 0.62) solid solution is formed by substitution of replacement of lanthanum atoms by erbium atoms with a smaller radii

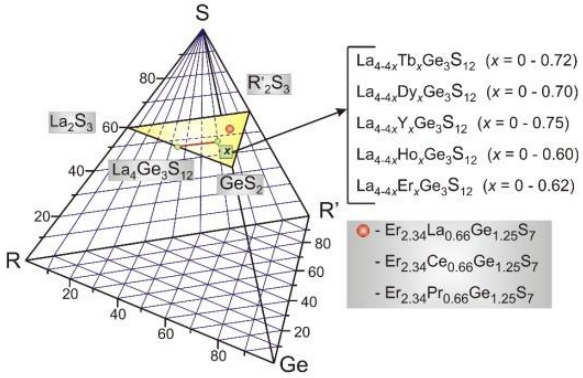

Fig. 2. The concentration tetrahedral of the La – R' – Ge – S (R' – Tb, Dy, Y, Ho, Er) sulfide system.

($r_{La^{+3}}/r_{Er^{+3}} = 1.14$ (Coordination surrounding (CS) = 8); $r_{La^{+3}}/r_{Er^{+3}} = 1.13$ (CS = 9), [12]). The same character of substitution is observed for other solid solutions:

$La_{4-4x}Tb_xGe_3S_{12}$ (x = 0 – 0.72; $r_{La^{+3}}/r_{Tb^{+3}} = 1.11$ (CS = 8); $r_{La^{+3}}/r_{Tb^{+3}} = 1.10$ (CS = 9)), $La_{4-4x}Dy_xGe_3S_{12}$ (x = 0 – 0.70; $r_{La^{+3}}/r_{Dy^{+3}} = 1.11$ (CS = 8), $r_{La^{+3}}/r_{Dy^{+3}} = 1.11$ (CS = 9)), $La_{4-4x}Y_xGe_3S_{12}$ (x = 0 – 0.75; $r_{La^{+3}}/r_{Y^{+3}} = 1.12$ (CS = 8), $r_{La^{+3}}/r_{Y^{+3}} = 1.11$ (CS = 9)) and $La_{4-4x}Ho_xGe_3S_{12}$ (x = 0 – 0.60; $r_{La^{+3}}/r_{Ho^{+3}} = 1.13$ (CS = 8), $r_{La^{+3}}/r_{Ho^{+3}} = 1.12$ (CS = 9)) [12].

The crystal structure ofsolid solutions $La_{4-4x}Tb_xGe_3S_{12}$ (x = 0 - 0.72), $La_{4-4x}Dy_{4x}Ge_3S_{12}$ (x = 0 - 0.70), $La_{4-4x}Y_{4x}Ge_3S_{12}$ (x = 0 - 0.75), $La_{4-4x}Ho_{4x}Ge_3S_{12}$ (x = 0 - 0.60) і $La_{4-4x}Er_{4x}Ge_3S_{12}$ (x = 0 - 0.62) is derived from the structure of the $La_4Ge_3S_{12}$compound (ST $La_4Ge_3S_{12}$; Symbol Pearson *hR*38; SG *R*3*c*). In the structure (Fig. 3) the site *6i* (0,0,0) and the 18*b* (x,y,z) are filled with statistical mixture of M1 (La + R) and M2 (R + La), respectively.

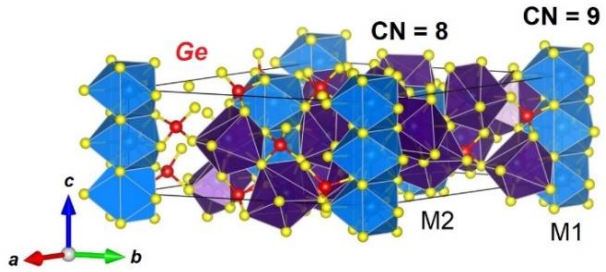

Fig. 3. The polihedra in the crystal structure of $La_{2,16}Er_{1,84}Ge_3S_{12}$ (M1 : 0,80 Er + 0,20 La) (M2 : 0,65 La + 0,35 Er).

The statistical mixture M1 (6*a*) are distinguished by a higher content of atoms R (R – Tb, Dy, Y, Ho або Er), and M2 (ПСТ 18*b*) – by a higher content of atoms La. The atoms are in the two type of polihedra: trigonal prism [M1 9S] with tree additional atoms S and trigonal prism [M2 8S] with two additional atoms S. The [Ge 4S] tetrahedral environment setting is for Ge atoms.

In Table 8, the volume, effective coordination environment settings and distortion index (DI) for trigonal prism [M1 9S] with tree additional atoms S and trigonal prism [M2 8S] with two additional atoms S of the $La_4Ge_3S_{12}$, $La_{2,02}Tb_{1,98}Ge_3S_{12}$, $La_{2,64}Dy_{1,36}Ge_3S_{12}$, $La_{2,25}Ho_{1,75}Ge_3S_{12}$ і $La_{2,16}Er_{1,84}Ge_3S_{12}$ composition are presented.

In the statistical mixture M1 (La + R) with a predominant content of Tb, Dy, Ho or Er atoms, a significant decrease in the volumes of trigonal prisms [M1 9S] compared to the volume of the trigonal prism [La 9S] is observed in the structure of $La_4Ge_3S_{12}$. Substitution of lanthanum atoms in trigonal [La 9S] prisms by Tb, Dy, Ho, or Er atoms causes an increase in the distortion index (DI). Hence, the trigonal [M1 9S] are less symmetrical compared to the trigonal [La 9S] prism in the structure of $La_4Ge_3S_{12}$.

In trigonal prisms M2 (La + R) with a predominant content of La atoms, the volume of trigonal prisms [M2 8S] decreases compared to the volume of trigonal prism [La 8S], but not significantly.

The decrease of volume of the trigonal [M1 9S] and [M2 8S] prisms correlates well with changes in the parameters of the cells in the structure of sulfides of $La_4Ge_3S_{12}$, $La_{2,02}Tb_{1,98}Ge_3S_{12}$, $La_{2,64}Dy_{1,36}Ge_3S_{12}$, $La_{2,25}Ho_{1,75}Ge_3S_{12}$ і $La_{2,16}Er_{1,84}Ge_3S_{12}$ (Fig. 5).

Table 8.

The parameters of [M1 9S] and [M2 8S] polihedra in the structure of sulfide: 1 – $La_4Ge_3S_{12}$, 2 – $La_{2,02}Tb_{1,98}Ge_3S_{12}$, 3 – $La_{2,64}Dy_{1,36}Ge_3S_{12}$, 4 – $La_{2,25}Ho_{1,75}Ge_3S_{12}$, 5 – $La_{2,16}Er_{1,84}Ge_3S_{12}$

Sulfide phase	[M1 9S]			[M2 8S]		
	V, nm^3	CS_{eff}	DI	V, nm^3	CS_{eff}	DI
$La_4Ge_3S_{12}$	0.05715	7.49	0.0677	0.04833	7.11	0.0440
$La_{2,02}Tb_{1,98}Ge_3S_{12}$	M1 = 0.13 La + 0.87 Tb			M2 = 0.63 La + 0.37 Tb		
	0.05321	7.01	0.0816	0.04644	7.15	0.0454
$La_{2,64}Dy_{1,36}Ge_3S_{12}$	M1 = 0.35 La + 0.75 Dy			M2 = 0.76 La + 0.24 Dy		
	0.05364	7.07	0.0801	0.04674	7.16	0.0443
$La_{2,25}Ho_{1,75}Ge_3S_{12}$	M1 = 0.22 La + 0.78 Ho			M2 = 0.68 La + 0.32 Ho		
	0.05296	6.98	0.0825	0.04621	7.14	0.0458
$La_{2,16}Er_{1,84}Ge_3S_{12}$	M1 = 0.20 La + 0.80 Er			M2 = 0.65 La + 0.35 Er		
	0.05233	6.90	0.0851	0.04582	7.14	0.0460

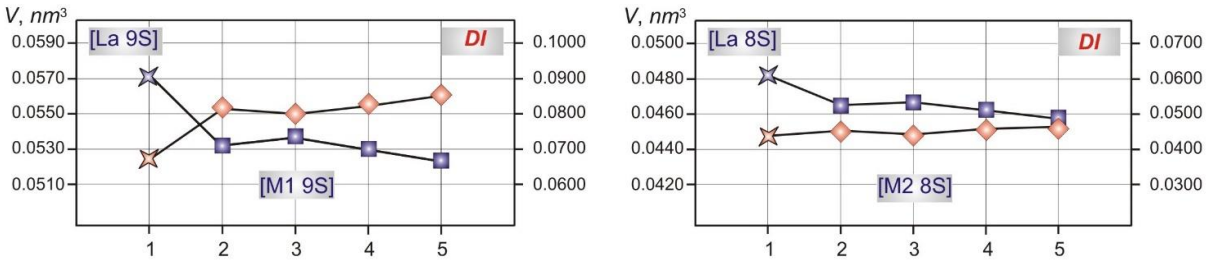

Fig. 4. The parameters of [M1 9S] and [M2 8S] polihedra (volume (V) and distortion index (DI)) for the sulfide structure: 1 – $La_4Ge_3S_{12}$, 2 – $La_{2,02}Tb_{1,98}Ge_3S_{12}$, 3 – $La_{2,64}Dy_{1,36}Ge_3S_{12}$, 4 – $La_{2,25}Ho_{1,75}Ge_3S_{12}$, 5 – $La_{2,16}Er_{1,84}Ge_3S_{12}$.

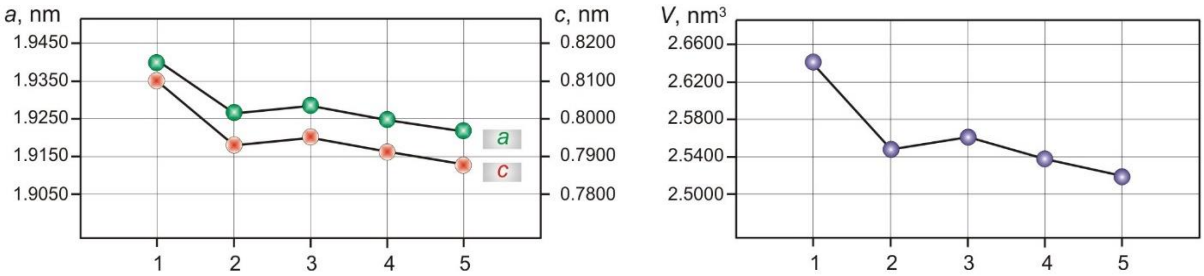

Fig. 5. The change of the lattice parameters of sulfide: 1 – $La_4Ge_3S_{12}$, 2 – $La_{2,02}Tb_{1,98}Ge_3S_{12}$, 3 – $La_{2,64}Dy_{1,36}Ge_3S_{12}$,
4 – $La_{2,25}Ho_{1,75}Ge_3S_{12}$, 5 – $La_{2,16}Er_{1,84}Ge_3S_{12}$.

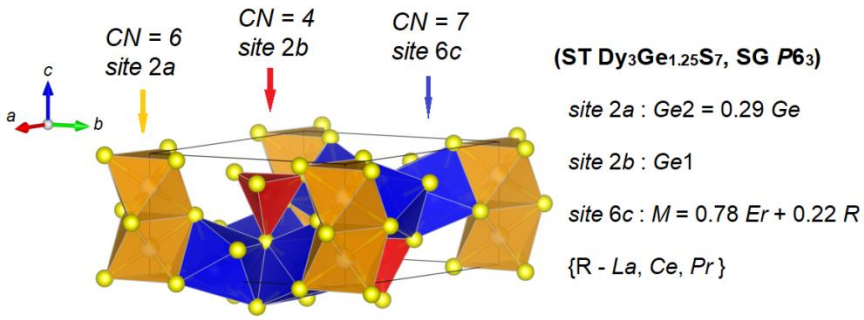

Fig. 6. The projection of cell and stacking of polyhedra in the structure of $Er_{2,34}La_{0,66}Ge_{1,25}S_7$, $Er_{2,34}Ce_{0,66}Ge_{1,25}S_7$ and $Er_{2,34}Pr_{0,66}Ge_{1,25}S_7$.

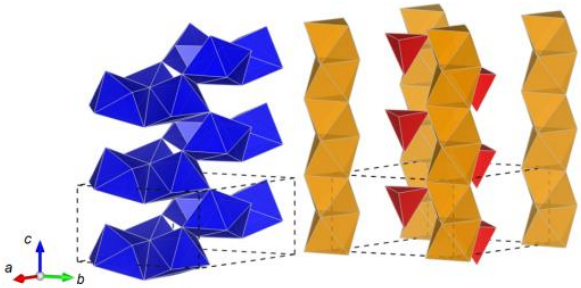

Fig. 7. "Blocks" and "columns" in the structure of $Er_{2,34}La_{0,66}Ge_{1,25}S_7$, $Er_{2,34}Ce_{0,66}Ge_{1,25}S_7$ and $Er_{2,34}Pr_{0,66}Ge_{1,25}S_7$.

Existence of sulfide $Er_{2,34}La_{0,66}Ge_{1,25}S_7$ phase was established for the first time during the study of phase equilibria in the Er_2S_3 – La_2S_3 – GeS_2 system at 770 K. The crystal structure of the phase investigated with single crystal method. The $Er_{2,34}Ce_{0,66}Ge_{1,25}S_7$ and $Er_{2,34}Pr_{0,66}Ge_{1,25}S_7$ phases are synthesized by isomorphic substitution of lanthanum atoms for cerium and praseodymium atoms, respectively. The phases are crystalized in hexagonal symmetry (ST $Dy_3Ge_{1,25}S_7$; Pearson Symbol *hP*23; SG $P6_3$).

In the structure of quaternary sylfides $Er_{2,34}La_{0,66}Ge_{1,25}S_7$, $Er_{2,34}Ce_{0,66}Ge_{1,25}S_7$ i $Er_{2,34}Pr_{0,66}Ge_{1,25}S_7$ the site 6*c* is filled with statistical mixture Er + La, Er + Ce and Er + Pr, respectively. Ge atoms are in the site 2*a* (Occ. = 0.29) and 2*b*. Atoms of the statistical mixture with sulfur atoms form trigonal prisms [M 7S] with one additional atom. These prisms form "blocks" (three prisms each), in which the prisms are connected to each other by common edges (Fig. 7). Ge atoms form two type of polihedra – tetrahedral and octahedral. [Ge2 6S] octahedra in the direction of the c axis form "columns" with common faces. The [Ge1 4S] tetrahedra are isolated from each other and are connected to the prism "blocks" by one vertex or three edges. All synthesized chalcogenides have a non-centrosymmetric crystal structure, and therefore are promising objects for nonlinear optical research.

Conclusions

In summary, substitution of rare earth elements in *R*3*c* quaternary $La_{4-4x}R_{4x}Ge_3S_{12}$ (R – Er, Ho, Y, Dy, Tb) sulfides offers a versatile approach to modify the crystal structure and properties of these materials for tailored applications across various fields. By understanding the interplay between substitution and material characteristics, researchers can design novel materials with enhanced functionalities and performance. Dysprosium is known for their strong magnetic properties. When the element is incorporated into a material, it can enhance its magnetic properties, making it more suitable for applications such as magnetic storage devices and sensors. Lanthanum can improve the electrical conductivity of a material. The addition of yttrium can improve the strength and toughness of a material, making it more suitable for structural applications. The physical properties of a material will depend on concentration of rare earth elements, distribution, and interactions with other elements in the material. In order to establish such relationships, it is necessary to carry out targeted research.

Smitiukh O. – Candidate of Chemical Sciences, Senior Lecturer of the Department of Inorganic and Physical Chemistry;
Marchuk O. – Candidate of Chemical Sciences, Associate Professor of the Department of Inorganic and Physical Chemistry.

[1] E. Ateia Ebtesam, M.A. Ahmed, and Rehab Ghouniem, *Effect of rare earth substitution on the structural and electrical properties of Cu–Mg ferrite*, International Journal of Modern Physics *B*. 29(19), 1550126 (2015); https://doi.org/10.1142/S021797921550126X.
[2] E. Newnham Robert, Properties of materials (Oxford University Press, New York, 2005); http://surl.li/rdfuz.
[3] M.Ya. Rudysh, O.V. Smitiukh, G.L. Myronchuk, S.M. Onedelnyk, O.V. Marchuk, *Band Structure Calculation and Optical Properties of Ag_3AsS_3 Crystals*, Physics and chemistry of solid state, 24(1), 17 (2023); https://doi.org/10.15330/pcss.24.1.17-22.
[4] Anatolii Fedorchuk, Yu. Grin, *Handbook on the Physics and Chemistry of Rare Earths*, 81 (2018); https://doi.org/10.1016/bs.hpcre.2018.04.002.
[5] George F. Harrington, Sunho Kim, Kazunari Sasaki, Harry L. Tullercd and Steffen Grieshammer, *Strain-modified ionic conductivity in rare-earth substituted ceria: effects of migration direction, barriers, and defect-interactions*, J. Mater. Chem. *A*, 9, 8630 (2021); https://doi.org/10.1039/D0TA12150A.
[6] Mohammad Basha, Morsi Mohamed, Morsi Morsi, Ahmad Fouad Basha, *The Magnetic, Electrical and Optical Properties of Rare Earth Er3+ Doped Lead Borate Glass*, Journal of Electronic Materials, 48(10), (2019); https://doi.org/10.1007/s11664-019-07487-x.
[7] L. Akselrud, Y. Grin, *WinCSD: Software package for crystallographic calculations (Version 4)*, J. Appl. Crystallogr., 47, 803 (2014); https://doi.org/10.1107/S1600576714001058.
[8] K. Momma, F. Izumi, *VESTA 3 for three-dimensional visualization of crystal, volumetric and morphology data*, J. Appl. Crystallogr., 44, 1272 (2011); https://doi.org/10.1107/S0021889811038970/FULL.
[9] O.V. Smitiukh, O.V. Marchuk, I.D. Olekseyuk, L.D. Gulay, *The Y_2S_3–La_2S_3–GeS_2 system at 770 K*, J. Alloys compd., 698, 739 (2017); https://doi.org/10.1016/j.jallcom.2016.12.283.
[10] O. Smitiukh, O. Marchuk, I. Olekseiuk, L. Hulay, O. Smitiukh, O. Marchuk, I. Olekseiuk, L. Hulay, The 16th Scientific Conference "Lviv Chemical Readings - 2017", May 28. (Lviv, 2017). In Ukrainian.
[11] M. Daszkiewicz, O.V. Smitiukh, O.V. Marchuk, L.D. Gulay, *The crystal structure of $Er_{2.34}La_{0.66}Ge_{1.28}S_7$ and the $La_xR_yGe_3S_{12}$ phases (R – Tb, Dy, Ho and Er)*, J. Alloys compd., 738, 263 (2018); https://doi.org/10.1016/j.jallcom.2017.12.207.
[12] J. Emsley. The Elements. 2nd edition (Oxford University Press, New York, 1991).

О. Смітюх, О. Марчук

Вплив заміщення рідкісноземельних металів на кристалічної структури та властивості тетрарних сульфідів $La_{4-4x}R_{4x}Ge_3S_{12}$ (R – Er, Ho, Y, Dy, Tb)

Волинський національний університет імені Лесі Українки, м. Луцьк, Українки, Smitiukh.Oleksandr@vnu.edu.ua

Встановлення взаємозв'язків між розподілом атомів в кристалічній комірці та властивостями фаз є важливою проблемою, що безпосередньо пов'язана із застосуванням функціональних матеріалів. У цій роботі нами представлено аналіз кристалічної структури, хімічних зв'язків та прогнозування характеру властивостей речовини на прикладі тетрарних фаз $La_{4-4x}R_{4x}Ge_3S_{12}$ (R – Er, Ho, Y, Dy, Tb), що кристалізуються в просторовій групі *R*3*c*. Важливим внеском в зміну властивостей, зокрема термоелектричних, є присутність рідкісноземемельних елементів з високою координацією першої координаційної сфери. Це створює можливість для підвищення ентропійного фактору і, як результат, сприяє покращенню термоелектричних характеристик. Параметри елементарної комірки вихідної тернарної фази $La_4Ge_3S_{12}$ зменшуються при співвідношенні 1La:1R (R – Tb, Dy, Ho, Er) в ПСТ 6*a* та 18*b*. В Er-вмісній фазі найнижчий дисторційних індекс для поліедра [M1 8S], в той час як в поліедрі [M1 9S] він значно зростає. Окрім того, утворення «колон» із поліедрів [Ge2 6S] створює можливість поступального збудження в одному із напрямків, що також може мати суттєвий вплив на властивості матеріалів. В цілому, отримані нецентросиметричні матеріали можуть бути перспективними для нелінійної оптики.

Ключові слова: досторційний фактор; кристалічна структура; рідкісноземельні метали; елементарна комірка; тетрарні сульфіди.